AIAA JOURNAL
Vol. 44, No. 4, April 2006

Feedback Control and Optimization for Rotating Disk Flutter Suppression with Actuator Patches

Xingzhe Wang*
Lanzhou University, 730000 Lanzhou, People's Republic of China
and
Xiaoyang Huang†
Nanyang Technological University, Singapore 639798, Republic of Singapore

An analytical study is presented on feedback control of rotating disk flutter by using piezoelectric patches as actuators. In this study, a thin disk is rotated in an enclosure, which is equipped with a feedback control loop consisting of a sensor, a signal processor, and several piezoelectric actuator patches. The actuator patches are mounted on the inner surface of the enclosure and produce necessary control force through the airflow around the disk. The dynamic stability of the disk-enclosure system, together with the feedback control loop, is analyzed as a complex eigenvalue problem, which is solved by the Galerkin's discretization procedure. The control performance, in terms of the control gain, the phase shift, and especially the configuration of the actuator patches, are evaluated by calculating the complex eigenvalues. The result shows that the disk flutter can be reduced effectively with proper combinations of the control gain and the phase shift with using one actuator patch or two/three patches. To achieve a high control performance, the suitable sizes and arrangements for several actuator patches distributed are optimized numerically.

Nomenclature

$A_j(r,\theta)$	=	distribution function of the control gain and phase shift for the jth actuator patch
a	=	speed of sound
$[\boldsymbol{B}]$	=	matrix associated with the free vibration of the rotating disk
C	=	nondimensional damping coefficient
c_m	=	coefficients for series expansion of w
$[\boldsymbol{c}]$	=	$[c_0 \;\; c_1 \;\; \cdots \;\; c_{M_0}]^T$
D	=	flexural stiffness
d_k^a	=	coefficients of Bessel series for ϕ_a
d_k^c	=	coefficients of Bessel series for ϕ_c
E	=	Young's modulus
G_j	=	gain of feedback control for the jth actuator patch
h	=	thickness of disk
M	=	Mach number at the disk outer edge
M_0	=	integer for maximum m for the simulation
m	=	integers for numbers of nodal circles
n	=	integers for numbers of nodal diameters
$[\boldsymbol{P}_a]$	=	matrix associated with acoustic force
$[\boldsymbol{P}_c]$	=	matrix associated with control force
$[\boldsymbol{P}_f]$	=	matrix associated with aerodynamic force
q_a	=	acoustic loading on disk
q_c	=	control-generated loading on disk
q_f	=	aerodynamic loading on disk
r	=	r component in cylindrical coordinate system
r_e	=	radius of the enclosure
r_i	=	radius of the clamping collar of the disk
r_s	=	r location of the sensor
r_0	=	radius of the disk
S_a	=	total area of the actuator patches
t	=	time
w	=	transverse displacement of the disk
z	=	z component in cylindrical coordinate system
z_e	=	distance from the upper surface of the enclosure to the disk
θ	=	θ component of the cylindrical coordinate system
θ_s	=	θ component of the cylindrical coordinate system for sensor
κ	=	r_i/r_0
Λ	=	mass ratio $\rho_a r_0/\rho_d h$
λ	=	eigenvalue
μ	=	$D/(\rho_d r_0^4 h\Omega^2)$
ν	=	Poisson ratio of disk
ρ_a	=	density of air
ρ_d	=	density of disk
σ_j	=	phase shift of feedback control for the jth actuator patch
σ_r	=	radial membrane stress of disk
σ_θ	=	hoop membrane stress of disk
ϕ_a	=	velocity potential associated with acoustic loading
ϕ_c	=	velocity potential associated with control generated loading
Ω	=	rotational speed of disk
Ω_d	=	rotational speed of damping force in aerodynamic loading

Received 10 July 2005; revision received 8 August 2005; accepted for publication 10 September 2005.

*Associate Professor, School of Civil Engineering and Mechanics, Gansu.
†Associate Professor, School of Mechanical and Production Engineering.

I. Introduction

ROTATING disk elements are widely used in various engineering applications, such as turbines, gyroscopes, annular saw blades, and data-storage recording systems. With rapid growth of the data-storage density and increase of the spindle motor speed in hard disk drivers (HDD), the stability of rotating disks is becoming an important issue because of its significant contribution to the track miss-registration and the disk drive failure. The disk rotating at a high speed can lose stability because of the coupling of the disk structure with surrounding airflow in such a way that energy is absorbed by the disk from airflow at a rate faster that that dissipated. This is called aeroelastic instability, or flutter.

The vibration of a rotating disk coupled with surrounding airflow has been of interest to many investigators in the past decades. Hosaka and Crandall,[1] Huang and Mote,[2] and Renshaw[3] studied the stability of a flexible floppy disk rotating very close to a rigid wall. Their analyses were based on the classical hydrodynamic lubrication theory to

describe the mechanism of the thin viscous flow in the gap coupling to the disk. Yasuda et al.[4] proposed a theoretical model in which the aerodynamic force exerted on a spinning disk was written in terms of "lift" and "damping" forces. They assumed that the ratio between the lift and damping force, which was equivalent to the speed of the damping force, was proportional to the rotation speed. Similar to the analysis for disks rotating close to a rigid wall, they showed that the flutter of a single backward traveling wave could appear at a certain rotation speed. D'Angelo and Mote[5] and Renshaw et al.[6] experimentally investigated the vibration of a thin disk rotating in atmospheres of different densities and observed the disk flutter and the flutter mode. Based on a generalized rotating damping model, Kim et al.[7] and Hansen et al.[8] respectively suggested a similar empirical model to predict flutter of a disk rotating in a fluid where the relationship between the speed of the disk and the damping force was estimated according to experimentally determined parameters.

The research activities in disk flutter have recently been directly related to hard disk drives. Imai et al.[9] and Imai[10] experimentally investigated the mechanism of disk flutter excitation in hard disk driver and suggested a technique by deceasing the disk-to-shroud spacing to reduce amplitudes of disk flutter. Heo et al.[11] presented another control method, which used a better aerodynamic design of the shroud contour on the base casting to reduce the disk flutter. Bittner and Shen[12] proposed an acoustically tuned-mass damper to suppress the disk flutter by an air bearing plate above the top disk. By employing a squeeze film damping to a commercially available HDD, Deeyiengyang and Ono[13] conducted experiments to study the effect of clearances between the squeeze film and the disk surface on suppressing vibration of the spinning disk/spindle system. All of these methods are passive control techniques, which either modified the configuration of the disk drive casings and aerodynamics of the disks or increased the dynamic damping of the disk.

Recently, Huang et al.[14,15] proposed an active control method to suppress the rotating disk flutter, in which the disk vibration signals were detected and processed to generate pressure perturbations inside the disk enclosure in such way that the original coupling would be altered and the disk flutter was therefore suppressed. This was shown theoretically by a dynamic stability study on a disk-air-enclosure system and experimentally by a disk rotating between two fixed plates. The feedback control systems generally require sensors and actuators, which are relatively easily to be implemented in modeling and laboratory experiments. However, in real hard disk drives, the actuators might be problems in applying the feedback control techniques because the spaces are limited there. In this paper, we propose to use piezoelectric patches as actuators and study the performance of control under various arrangement of a number of actuator patches. The thin piezoelectric patches are attached on the cover plate surface of the enclosure, and vibrations of these actuator patches generate the control forces by the disturbed acoustic field in the disk-enclosure system. By taking into account the air-coupling and control force on the rotating disk, the dynamic stability of the rotating disk is analyzed using the Galerkin's method. It is demonstrated that, with a proper combination of the control gain and phase shift, the disk flutter can be suppressed effectively by one actuator patch, two actuator patches, and three actuator patches distributed on the cover plate surface of the enclosure. An optimization performance study in terms of sizes and arrangements of the actuator patches is also conducted.

II. Theoretical Modeling and Formulation

Consider an annular disk with a uniform thickness h and outer radius r_0, clamped at the center with radius r_i in a cylindrically shaped enclosure, as shown in Fig. 1. The disk rotates about its symmetry axis at a constant angular speed Ω. The material parameters of the disk, Young's modulus, Poisson's ratio, and density are E, ν, and ρ_d, respectively. The enclosure has radius r_e and height $2z_e$, and the density of air in the enclosure is ρ_a. The rotating disk with small transverse motions is modeled by the linear Kirchhoff plate theory with in-plane stresses. The governing equation in terms of the transverse displacement $\bar{w}(\bar{r}, \theta, \bar{t})$, with respect to the space-fixed coordinates $(\bar{r}, \theta, \bar{z})$, can be written in a nondimensional form as follows[3,6,8,14]:

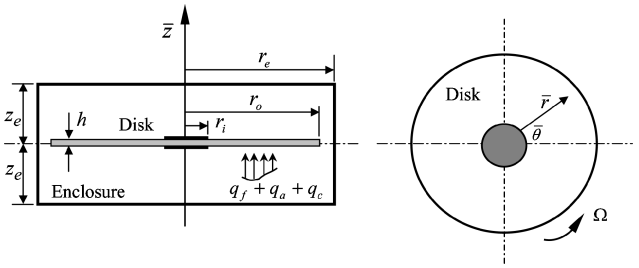

Fig. 1 Geometry of disk and cylindrical enclosure.

$$\frac{\partial^2 w}{\partial t^2} + 2\frac{\partial^2 w}{\partial t \partial \theta} + \frac{\partial^2 w}{\partial \theta^2} + \mu \nabla^4 w - \left[\frac{1}{r}\frac{\partial}{\partial r}\left(r\sigma_r \frac{\partial w}{\partial r}\right) + \frac{1}{r^2}\frac{\partial}{\partial \theta}\left(\sigma_\theta \frac{\partial w}{\partial \theta}\right)\right] = q(r, \theta, t) \tag{1}$$

where

$$w = \frac{\bar{w}}{h}, \qquad r = \frac{\bar{r}}{r_0}, \qquad z = \frac{\bar{z}}{r_0}, \qquad t = \Omega \bar{t}, \qquad \kappa = \frac{r_i}{r_0}$$

$$\sigma_r = \frac{\bar{\sigma}_r}{\rho_d r_0^2 \Omega^2}, \qquad \sigma_\theta = \frac{\bar{\sigma}_\theta}{\rho_d r_0^2 \Omega^2}, \qquad q = \frac{\bar{q}}{\rho_d h^2 \Omega^2} \tag{2}$$

$\mu = D/\rho_d r_0^4 \Omega^2 h$ is the ratio of the disk bending stiffness to the stiffness derived from the centrifugal body force of rotation, $D = Eh^3/12(1-\nu^2)$ is the flexibility rigidity of the disk, and $\nabla^4 = (\partial^2/\partial r^2 + \partial/r\partial r + \partial^2/r^2\partial\theta^2)^2$ is the biharmonic differential operator. Here $q(r, \theta, t)$ represents the transverse loading acted on the rotating disk, which includes aerodynamic force $q_f(r, \theta, t)$, acoustic force $q_a(r, \theta, t)$, and control force $q_a(r, \theta, t)$. Here σ_r and σ_θ are the radial and hoop membrane stresses, satisfying the generalized plane-stress equations of linear elasticity with a centrifugal body force.[16] Equation (1) formulates the vibration motion of the rotating disk, together with the boundary conditions at the clamped and free edges of the disk,

$$w|_{r=\kappa} = 0, \qquad \left.\frac{\partial w}{\partial r}\right|_{r=\kappa} = 0 \tag{3a}$$

$$D\left[\frac{\partial^2 w}{\partial r^2} + \nu\left(\frac{1}{r}\frac{\partial w}{\partial r} + \frac{1}{r^2}\frac{\partial^2 w}{\partial \theta^2}\right)\right]_{r=1} = 0$$

$$D\left[\frac{\partial}{\partial r}(\nabla^2 w) + \frac{(1-\nu)}{r^2}\frac{\partial^2}{\partial \theta^2}\left(\frac{\partial w}{\partial r} - \frac{w}{r}\right)\right]_{r=1} = 0 \tag{3b}$$

as well as the additional condition of circumferential periodicity, $w(r, \theta, t) = w(r, \theta + 2\pi, t)$.

A. Aerodynamic Force and Acoustic Force

The hydrodynamic model, based on the rigorous Navier–Stokes equations, for the description of the aerodynamic force arising from the airflow of the disk rotation is highly complicated to provide an analytical design. Here, the empirical model of aerodynamic force, generalized by Kim et al.[7] and Hansen et al.,[8] is employed in the study for the aerodynamic force. The model is based on a simple mechanism that takes the aerodynamic loading exerted on the disk as a distributed viscous damping force rotating relative to the disk. It has some inherent benefits for complex system analysis with avoidance of seeking the solution of the complete Navier–Stokes equations, but gives a good prediction on the rotating disk flutter qualitatively (see Refs. 14 and 15). The aerodynamic force $q_f(r, \theta, t)$ derived from this model is expressed as

$$q_f(r, \theta, t) = -C\left[\frac{\partial w}{\partial t} + \left(1 - \frac{\Omega_d}{\Omega}\right)\frac{\partial w}{\partial \theta}\right] \tag{4}$$

where C is a damping coefficient depending on the viscosity of the fluid, the rotational speed of the disk and the geometrical parameters of the enclosure, and Ω_d is the rotational speed of the distributed viscous damping force relative to the disk, which can be determined from experiments.[15]

The acoustic force $q_a(r, \theta, t)$ on the disk, arising from the acoustic pressure induced in the enclosure by the disk vibrations, can be calculated through the pressure difference between the upper and lower surfaces of the disk and can be written as

$$q_a(r, \theta, t) = \Lambda \left[\frac{\partial \phi_a(r, \theta, z = 0^+, t)}{\partial t} - \frac{\partial \phi_a(r, \theta, z = 0^-, t)}{\partial t} \right] \quad (5)$$

in which ϕ_a is the acoustic velocity potential. The governing equation for the acoustic field in the enclosure is expressed by

$$\bar{\nabla}^2 \phi_a = M^2 \frac{\partial^2 \phi_a}{\partial t^2} \quad (6)$$

where $\bar{\nabla}^2 = \partial^2/\partial r^2 + (1/r)(\partial/\partial r) + (1/r^2)(\partial^2/\partial \theta^2) + \partial^2/\partial z^2$ is the space Laplacian operator and $M = r_0\Omega/a$ is the Mach number at the outer edge of the disk. The boundary conditions on the upper and bottom plate surfaces and the sidewall of the enclosure are

$$\left.\frac{\partial \phi_a}{\partial r}\right|_{r=r_e} = 0, \qquad \left.\frac{\partial \phi_a}{\partial z}\right|_{z=\pm z_e} = 0 \quad (7a)$$

Here, $r_e = \bar{r}_e/r_0$, and $z_e = \bar{z}_e/r_0$. In addition, on the surface of the disk the acoustic velocity should match the disk vibration velocity. At the clearance between the disk rim and the enclosure sidewall, there is the antisymmetric condition $\phi_a = 0$ (Ref. 3):

$$\left.\frac{\partial \phi_a}{\partial z}\right|_{z=0} = \begin{cases} 0 & (0 \le r < \kappa) \\ \dfrac{\partial w}{\partial t} & (\kappa \le r \le 1) \end{cases}, \quad \phi_a|_{z=0} = 0 \; (1 < r \le r_e) \quad (7b)$$

There exhibits the acoustic-structure coupling between the disk vibration and the acoustic field via the velocity matching.

B. Control Force Induced by Actuator Patches

In the present study, the feedback control force is generated by actuator patches, which are attached on the cover plate surface of the enclosure. The configuration of these actuator patches, denoted by an integer $j = 1, 2, \ldots, J$, is shown in Fig. 2. A sensor is placed in the enclosure to peak up the disk vibrations at a fixed point (r_s, θ_s). The signals measured are then amplified and phase shifted to drive the actuator patches whose vibrations produce acoustic pressures inside the enclosure to act as the control forces. The actuator patches are arranged in three configurations, shown in Fig. 3. The actuating area on the covering plate is denoted as $S_a (= S_1 \cup S_2 \cup \cdots \cup S_J)$, and a distribution function for each patch is denoted as $A_j(r, \theta)$ $(j = 1, 2, \ldots, J)$ by

$$A_j(r, \theta) = \begin{cases} G_j e^{i\sigma_j} & [(r, \theta) \in S_j] \\ 0 & [(r, \theta) \notin S_j] \end{cases} \quad (8)$$

where G_j and σ_j are the control gain and the phase shift related to the jth actuator patch.

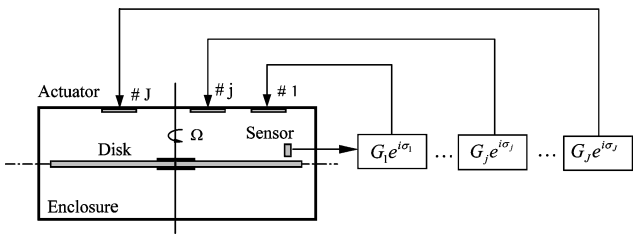

Fig. 2 Schematic diagram of feedback control with actuator patches.

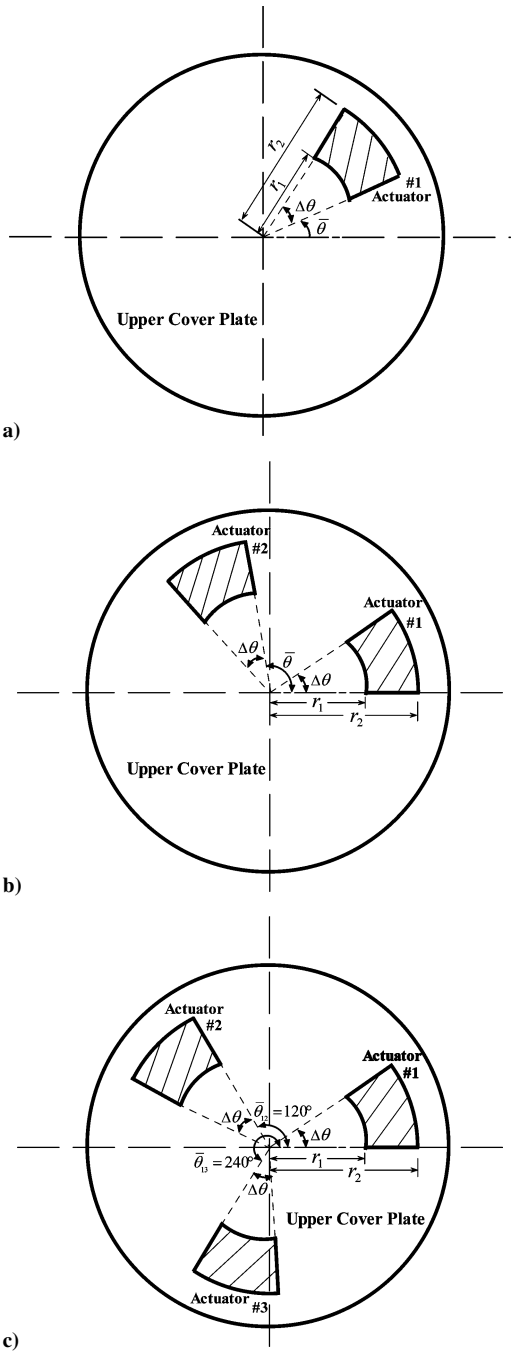

Fig. 3 Arrangement of actuator patch(es) distributed on the cover plate surface of the enclosure: a) one patch, b) two patches, and c) three patches.

The controlled acoustic field generated by these actuator patches, denoted by the velocity potential ϕ_c, is given by the following governing equation and boundary conditions:

$$\bar{\nabla}^2 \phi_c = M^2 \frac{\partial^2 \phi_c}{\partial t^2} \quad (9)$$

$$\left.\frac{\partial \phi_c}{\partial z}\right|_{z=0} = 0, \qquad \left.\frac{\partial \phi_c}{\partial r}\right|_{r=r_e} = 0 \quad (10a)$$

$$\left.\frac{\partial \phi_c}{\partial z}\right|_{z=z_e} = \begin{cases} A_j(r, \theta) \left.\dfrac{\partial w}{\partial t}\right|_{(r_s, \theta_s)} & [(r, \theta) \in S_j, \; j = 1, 2, \ldots, J] \\ 0 & [(r, \theta) \notin S_a] \end{cases} \quad (10b)$$

The control force generated on the disk surface can be calculated by

$$q_c(r,\theta,t) = \Lambda \frac{\partial \phi_c(r,\theta,z=0^+,t)}{\partial t} \tag{11}$$

By adding up together the aerodynamic force $q_f(r,\theta,t)$, the acoustic force $q_a(r,\theta,t)$, and the controlled force $q_c(r,\theta,t)$, the total loading acted on the rotating disk is therefore

$$q(r,\theta,t) = q_f(r,\theta,t) + q_a(r,\theta,t) + q_c(r,\theta,t) \tag{12}$$

As such, the governing equations (1), (6), and (9) and the corresponding boundary conditions describe the aeroelastically dynamic problem of a rotating disk in an enclosure involved the feedback control.

III. Numerical Analysis Procedure

The rotating disk vibration equation (1) will be solved together with all forces and the boundary conditions. All of the equations for the rotating disk and acoustic fields should be solved synchronously. The separable forms for the transverse displacement $w(r,\theta,t)$, and the acoustic velocity potentials $\phi_a(r,\theta,z,t)$ and $\phi_c(r,\theta,z,t)$, are assumed by

$$w(r,\theta,t) = R(r)\exp[i(n\theta+\lambda t)] \tag{13a}$$

$$\phi_a(r,\theta,z,t) = \psi_a(r,z)\exp[i(n\theta+\lambda t)]$$

$$\phi_c(r,\theta,z,t) = \psi_c(r,z)\exp[i(n\theta+\lambda t)] \tag{13b}$$

where $R(r)$, $\psi_a(r,z)$, and $\psi_c(r,z)$ are unknown functions to be determined. We can approximate $R(r)$ by the superposition of a series of linearly independent polynomials $R_{mn}(r)$ (Ref. 17) and rewrite the transverse displacement as

$$w(r,\theta,t) = \sum_{m=0}^{\infty} c_m R_{mn}(r)\exp[i(n\theta+\lambda t)] \tag{14}$$

where m and n represent the numbers of nodal circle and diameter for the disk vibration mode (m,n). In the numerical simulations, the infinite series can be truncated at $m = M_0$ within the allowable accuracy.

The acoustic velocity potentials ϕ_a and ϕ_c, which satisfy the governing equations (6) and (9) and the boundary conditions (7a) and (10a), can be solved as

$$\phi_a = \sum_{k=1}^{\infty} d_k^a \cosh[\alpha_k(z_e - z)] J_n(\xi_k r)\exp[i(n\theta+\lambda t)]$$

$$\phi_c = \sum_{k=1}^{\infty} d_k^c \cosh(\alpha_k z) J_n(\xi_k r)\exp[i(n\theta+\lambda t)] \tag{15}$$

where $J_n(\xi_k r)$ is the first kind of Bessel function of the nth order, ξ_k are the roots of $\mathrm{d}J_n(\xi_k r_e)/\mathrm{d}r = 0$ $(k = 1, 2, \ldots \infty)$, which is the boundary condition at the rigid sidewall of the enclosure, and $\alpha_k = \sqrt{(\xi_k^2 - M^2\lambda^2)}$. The coefficients d_k^a and d_k^c could be determined by the left boundary conditions of the velocity matching at $z = 0$ in Eq. (7b) and at $z = z_e$ in Eq. (10b), respectively. Owing to the couplings between the disturbed acoustic fields and the disk vibrations, they are functions of the coefficients c_m. That is, $d_k^a = d_k^a(c_m)$ and $d_k^c = d_k^c(c_m)$.

An approximation method based on Galerkin's discretization procedure is suggested to solve the problem. By substituting Eqs. (14) and (15) into the motion equation (1) of the rotating disk and calculating the inner product with $R_{ln}(r)e^{in\theta}$, $(l = 0, 1, \ldots M_0)$, one can obtain a matrix equation:

$$\{[\boldsymbol{B}] + [\boldsymbol{P}_f]\}[\boldsymbol{c}] + [\boldsymbol{q}_a([\boldsymbol{c}])] + [\boldsymbol{q}_c([\boldsymbol{c}])] = [0] \tag{16}$$

where $[\boldsymbol{c}] = [c_0 \;\; c_1 \;\; \cdots \;\; c_{M_0}]^T$ is an unknown coefficient matrix, $[\boldsymbol{B}]$ is a matrix with order of $(M_0+1) \times (M_0+1)$ associated with the free vibration of the rotating disk without any loading, $[\boldsymbol{P}_f]$ is a matrix of $(M_0+1)\times(M_0+1)$ order associated with the aerodynamic force caused by air-coupling, and $[\boldsymbol{q}_a([\boldsymbol{c}])]$ and $[\boldsymbol{q}_c([\boldsymbol{c}])]$ are, respectively, related to the acoustic force induced by the vibrations of the disk and control force by the vibrations of the actuator patches. They can be decomposed by a discretization arithmetic to resolve the coefficient matrix $[\boldsymbol{c}]$ explicitly as the following forms:

$$[\boldsymbol{q}_a([\boldsymbol{c}])] = [\boldsymbol{P}_a][\boldsymbol{c}], \qquad [\boldsymbol{q}_c([\boldsymbol{c}])] = [\boldsymbol{P}_c][\boldsymbol{c}] \tag{17}$$

The more details of the derivation are given in the Appendix. So, Eq. (16) is further reduced to a linear homogeneous equation. There exists the nontrivial solution only when the determinant of the coefficient matrix is equal to zero. It leads to a characteristic equation:

$$\det\{[\boldsymbol{B}] + [\boldsymbol{P}_f] + [\boldsymbol{P}_a] + [\boldsymbol{P}_c]\} = 0 \tag{18}$$

The eigenvalue λ can be obtained from the roots of the preceding equation. These roots come in (M_0+1) pairs and generate (M_0+1) pairs eigenvalues for a fixed nodal diameter n. Each pair of the eigenvalues is denoted by λ^{FTW} and λ^{BTW}, which, respectively, correspond to the forward traveling wave (FTW) and backward traveling wave (BTW) along and against the rotation direction of the disk.[4,7] The real parts of the eigenvalues $\mathrm{Re}(\lambda)$ are related to the mode frequencies of the disk vibration, whereas the imaginary parts $\mathrm{Im}(\lambda)$ are related to the damping of the disk vibration, and especially $\mathrm{Im}(\lambda) < 0$ indicates an unstable vibration or flutter, where the amplitude of the disk vibration will grow in time. If the disk rotates in a vacuum, all of the eigenvalues are real numbers, and the rotating disk system is therefore stable. Otherwise, when the disk rotates in air without the feedback control, the eigenvalues will be complex numbers, and for some modes above certain rotation speed $\mathrm{Im}(\lambda)$ will be negative, and the disk flutter occurs. By introducing the feedback control force $[\boldsymbol{q}_c]$ of the last term on the left-hand side in Eq. (16), or $[\boldsymbol{P}_c]$ in Eq. (18), we can expect the eigenvalues of the disk-enclosure system to be influenced so that the original aeroelastic stability of system will be altered and improved.

IV. Results and Discussion

Case studies are conducted in this section to show that it is possible to suppress flutter by the feedback control technique with one actuator patch or several patches. The material and geometrical properties of the disk are listed in Table 1, the same as the ones used by D'Angelo and Mote.[5] The parameters of the enclosure dimension are taken as $z_e = 0.5$ and $r_e = 1.2$, and the sensor to pick up the disk vibration is located at a point $(r_s, \theta_s) = (0.9, 0)$. In the simulation, we take $C = 0.02$ and $\Omega_d/\Omega = \frac{2}{3}$ for the aerodynamic loading exerted on the rotating disk.[14]

First, for the verification of the numerical program, the free vibration of a rotating disk in the enclosure without control is examined. The split natural frequencies of FTW and BTW modes, as well the critical speeds for the rotating disk at which some of BTW mode frequencies become zero, are evaluated. The prediction results, illustrated in Fig. 4a, are in good agreement with the experimental data. The critical speed predicted for mode (0, 3) in the present study is 2110 rpm, which is comparable to the 2078 rpm measured in Ref. 5 with an error about 1.5%. The eigenvalues of

Table 1 Geometrical and material property of the disk system

Parameter	Value
Outer radius r_0, m	0.178
Clamped radius r_i, m	5.34×10^{-2}
Thickness h, m	7.75×10^{-4}
Density of disk ρ_d, kg/m^3	7.84×10^3
Young's modulus E, MPa	2.0×10^5
Poisson's ratio ν	0.3
Density of air ρ_a, kg/m^3	1.21
Speed of sound in air a, m/s	3.4×10^2

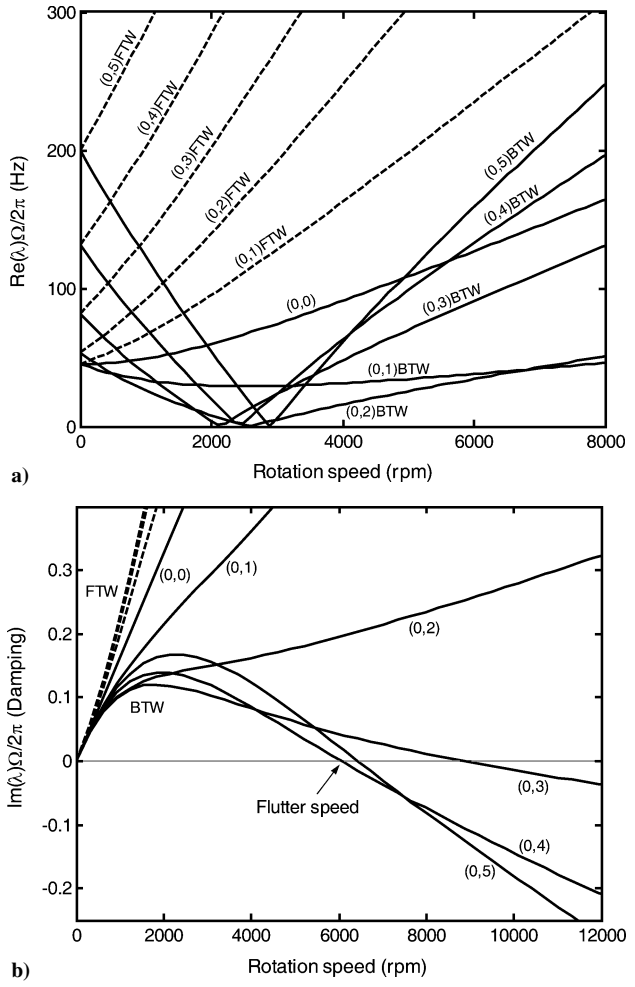

Fig. 4 Disk vibration in the enclosure beyond control: a) real part of the eigenvalue Re(λ) or mode frequency and b) imaginary part of the eigenvalue Im(λ) or system damping.

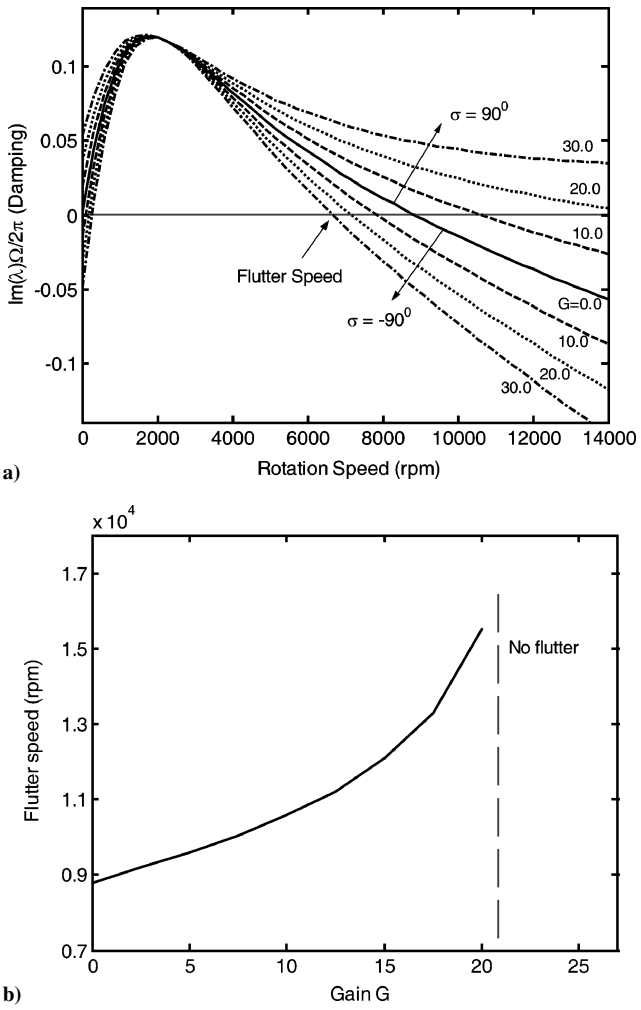

Fig. 5 Performance of flutter suppression on mode (0, 3) in one patch case with sector angle $\Delta\theta$ = 10 deg and relative angle $\bar{\theta}$ = 0 deg: a) Im(λ) vs rotation speed for different gains and phase shifts and b) flutter speed vs control gain for phase shift σ = 90 deg.

the disk-enclosure system are complex numbers whose real parts indicate the mode frequencies and the imaginary parts are related to the damping of the disk vibration. Figure 4b shows the damping of the disk vs the disk rotation speed. It is seen that these dampings are initially positive and then turn to negative, as the rotation speed increases, for some vibration modes such as (0, 3), (0, 4), and (0, 5) of BTW. The negative damping indicates the occurrence of flutter. The rotation speed at which the disk flutter takes place is called flutter speed, and the corresponding vibration mode is called flutter mode.

Secondly, the feedback control for suppressing the disk flutter is conducted. Several actuator patches shaped as annulus sectors are utilized in the control system (as illustrated in Fig. 3). The flutter suppression is fulfilled by introducing the control force $[\boldsymbol{P}_c]$ in the eigenvalue-problem equation. The control performance in terms of the sizes and arrangements of the actuator patches, along with the relative phase shift of the actuating policy design of the patches, is analyzed. The optimization design on the configuration of the actuator patches is investigated numerically to achieve a high control performance. All of these are presented in the following three case studies.

A. Case A: One Actuator Patch

As a simple case, the actuating system with one actuator patch (as shown in Fig. 3a) is studied to show the control performance and the optimization of the patch size for multiple flutter modes. The inner and outer radii of annulus sector patches are set as $r_1 = 0.7$ and $r_2 = 1.0$ (normalized by the disk outer radius r_0) in the following simulations unless a special annotation indicated.

The effect of the feedback control on the damping of the disk vibration that is, the imaginary part of eigenvalue, is shown in Fig. 5a for the flutter mode (0, 3), which is presented as the damping vs the rotating speed for various control gains and phase. One can see that the damping curves are lifted up for a proper phase shift $\sigma = 90$ deg, and the corresponding flutter speeds are increased. The stability of the rotating disk is therefore improved. On the other hand, it is illustrated that the feedback control can decrease the stability of the disk with an improper phase shift $\sigma = -90$ deg. From Fig. 5a, it is seen that the whole damping curve is positive when $\sigma = 90$ deg and the control gain is greater than 30, which means that the mode (0, 3) under this control setting is totally free from flutter. Figure 5b shows that the flutter speed of mode (0, 3) varies with the control gain for phase shift fixed at $\sigma = 90$ deg and the results illustrated that the flutter speed is gradually increased with increase of the gain, until the gain is greater than 20, at which the flutter speed is too high to have the flutter occur in practical disk operations. To take a close view on the performance of the feedback control depending upon the control parameters, the stability map in $G-\sigma$ plane for different rotation speeds is plotted in Fig. 6a. The stability map consists of a stable region in which $\mathrm{Im}(\lambda) > 0$, and an unstable region in which $\mathrm{Im}(\lambda) < 0$. One can find that the control system has a relative larger stable operation region with the combination of gain G and phase shift σ. This indicates that the feedback control is robust because the parameters of control can be chosen in a continuous region rather than at some isolated points or lines, or several discontinuous patch domains. The performance of the controller to other flutter modes, such as modes (0, 4) and (0, 5), is also examined, and the results

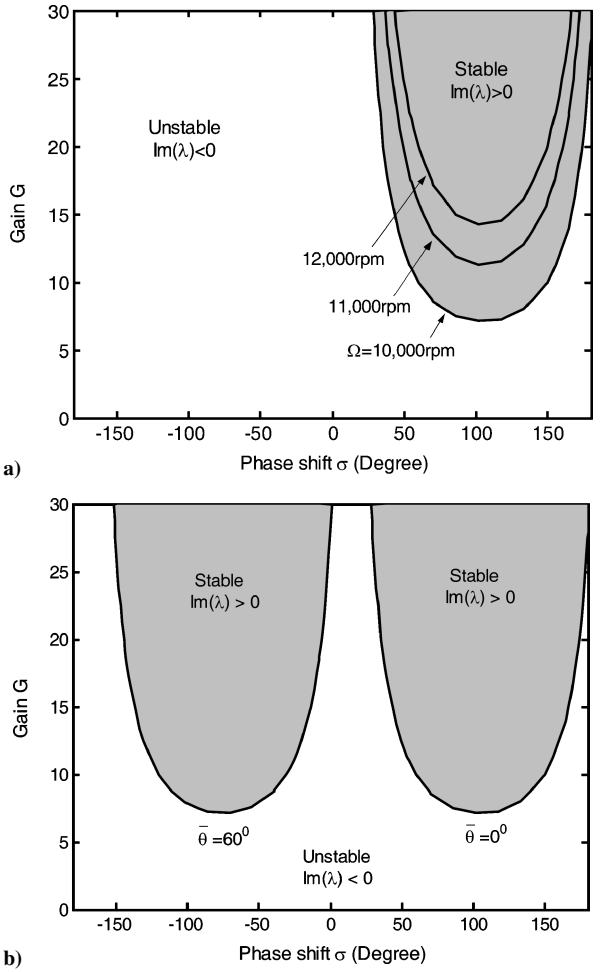

Fig. 6 Stability map of control for flutter mode (0, 3) in one patch case with sector angle $\Delta\theta$ = 10 deg: a) for different rotation speeds with $\bar{\theta}$ = 0 deg and b) for different relative location angle with disk rotation speed Ω = 10,000 rpm.

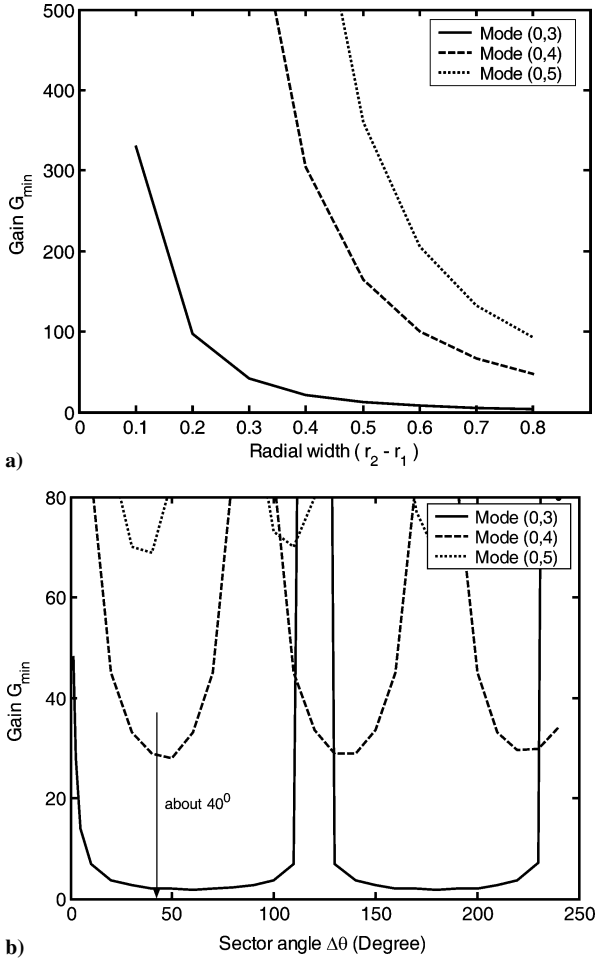

Fig. 7 Effect of actuator patch size on minimum gain of flutter suppression in one-patch case with disk rotation speed Ω = 10,000 rpm: a) by increasing radial width with a fixed sector angle $\Delta\theta$ = 10 deg (r_1 = 0.3) and b) by increasing sector angle with a fixed radial width.

are similar to those for mode (0, 3). The effect of the actuator patch location, in terms of $\bar{\theta}$, on the stability map is shown in Fig. 6b. It shows that the different patch locations have the same size of the stable area, though they are located in different region of the stability map.

The effect of the actuator patch size on the control performance is studied by plotting the minimum control gain vs $(r_2 - r_1)$ of the annulus sector with a fixed sector angle $\Delta\theta$ and vs $\Delta\theta$ with fixed $(r_2 - r_1)$. The results are shown in Figs. 7a and 7b, respectively. It is seen that, by increasing the radial width $(r_2 - r_1)$ of the annulus sector, the enlarged actuator generates a greater control force so that the required control gain is decreased, depicted by Fig. 7a for some modes. However, the effect of enlarging the actuator size through increasing $\Delta\theta$ is more complicated, as shown in Fig. 7b. One can find that there exhibits the periodic characteristics for the control, and some choices of the sector angles will lead to control invalidation. For instance, the control gains will tend to infinite as $\Delta\theta$ equals around 120 deg for flutter mode (0, 3), 90 and 180 deg for mode (0, 4), and around 72, 144, and 216 deg for mode (0, 5). That is, if the sector angle of the actuator patch is set as such values just shown, the disk flutters for the corresponding flutter modes will not be reduced whatever the phase shift is set. More attention should be paid to the actuator patch size design in the feedback control. The periodic feature and the control performance relying on the flutter mode can be explained by the control force dependence upon the nodal diameter of the vibration mode. With certain $\Delta\theta$ values, such as $\Delta\theta = 40$ deg, the required control gains are small, and the control is effective. While at some $\Delta\theta$ values, such as around $\Delta\theta = 20$ and 90 deg, the required control gains are much larger, and the control might not function. Certain values of $\Delta\theta$ can be good for one mode and not good for others. It is seen that if the control is set at $\Delta\theta = 40$ deg and $G = 70$, all three modes will be under control. It is the optimal sector angle for the patch size in the case of one actuator patch used in the actuating system.

B. Case B: Two Actuator Patches

In this case, the two actuator patches are of the same shape and actuating area, but they are separated by a relative location angle $\bar{\theta}$ between them, as depicted in Fig. 3b. The two actuators are actuated with the same control gain $G_1 = G_2$ and the phase shift $\sigma_1 = \sigma_2$. The effect of the actuator patch area on the control performance is studied by changing the sector angle $\Delta\theta$ from 5 to 90 deg and fixing $\bar{\theta} = 90$ deg, and the results of the minimum control gain vs $\Delta\theta$ are shown in Fig. 8a. It is seen that the sector angle does not have much effect on control of mode (0, 3), but for modes (0, 4) and (0, 5) the sector angle should be in a range around 40 deg, indicating that the larger actuating area does not always lead to a better control performance. The results show that, in case of two actuator patches, the optimal sector angle should be $\Delta\theta = 40$ deg to achieve effective flutter control for all three modes.

By keeping the size of each actuator patch as a constant, the effect of the relative location angle $\bar{\theta}$ between the two patches on the gains for multiple flutter modes suppression is plotted in Fig. 8b. Here the sector angle of each patch is set as $\Delta\theta = 20$ deg. A periodic characteristic for the effectiveness of flutter control is shown again in Fig. 8b. For the arrangements of the actuator patches located on the surface of the cover plate, like $\bar{\theta} = 60$ deg, 180 deg for flutter mode (0, 3), $\bar{\theta} = 45$ deg, 135 deg for mode (0, 4), and $\bar{\theta} = 110$ deg, 180 deg

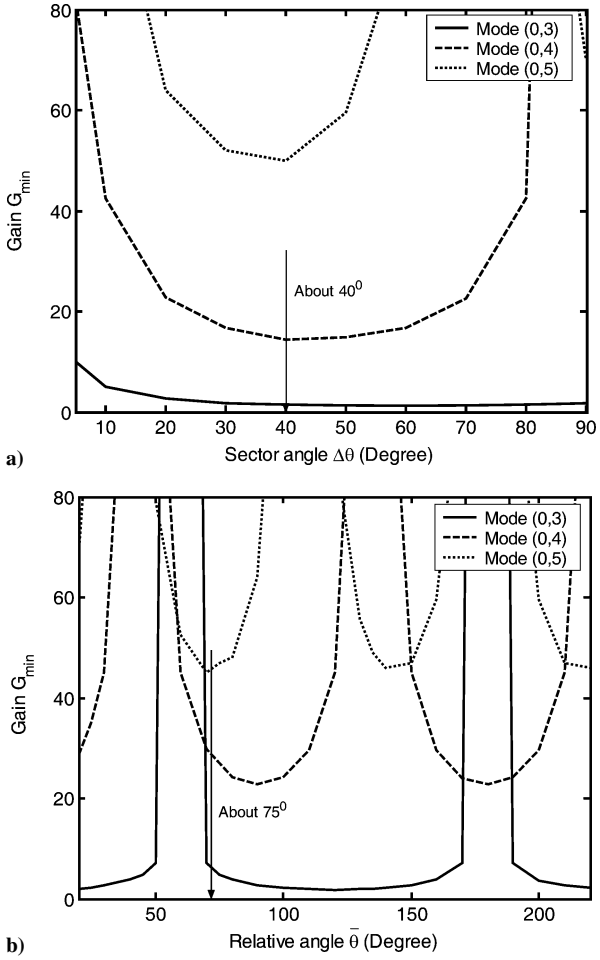

Fig. 8 Performance of flutter suppression in two-patch case with disk rotation speed Ω = 10,000 rpm: a) by increasing sector angle ($\bar{\theta}$ = 90 deg) and b) by changing relative location angle ($\Delta\theta$ = 20 deg).

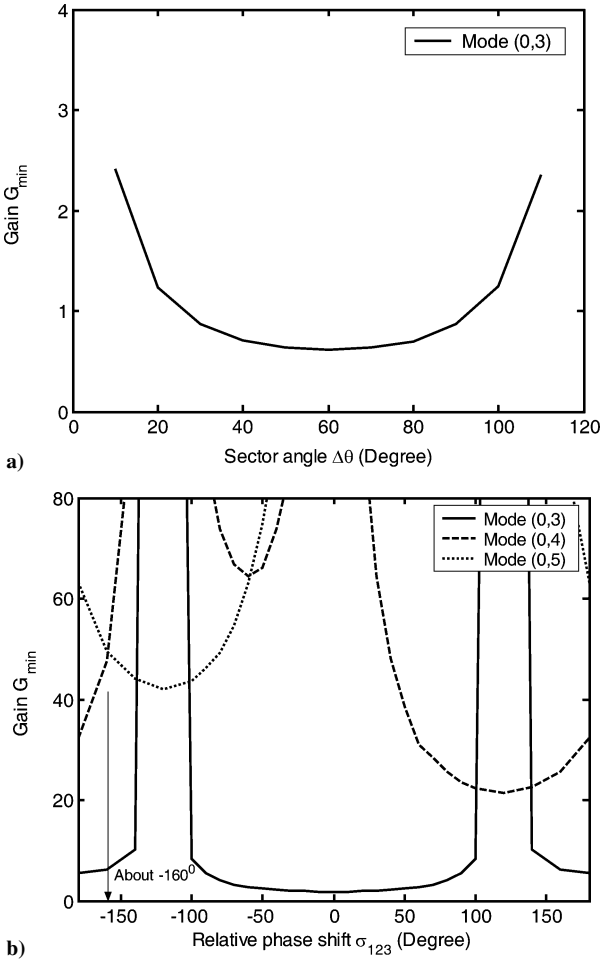

Fig. 9 Performance of flutter suppression in three-patch case with disk rotation speed Ω = 10,000 rpm: a) by increasing sector angle and b) by changing relative phase shift σ_{123} among patches ($\Delta\theta$ = 40 deg/3).

for mode (0, 5), the control gains trend to infinities, which means the flutter out of control. Such arrangements should be avoided for the location design of the patches in the implement of the feedback control. When the two patches are arranged with a relative location angel of $\bar{\theta} = 75$ deg, a high performance for the minimum gains of the flutter modes from (0, 3) to (0, 5) can be obtained. We notice that each actuator patch has sector angle of $\Delta\theta = 20$ deg, and the total area of the patches is the same as the optimal area of the one actuator patch case, that is, $\Delta\theta = 40$ deg. But it is found, in comparison the results with the ones of the one patch case as shown in Fig. 7b, that the minimum control gain is reduced obviously by 32.3% for the higher flutter mode (0, 5) and little differences on modes (0, 3) and (0, 4). In other words, if one actuator patch is divided into two patches arranged with a proper relative angle, a good performance of the flutter suppression, especially for the high flutter mode, can be achieved.

C. Case C: Three Actuator Patches

The three actuator patches distributed on the cover plate surface are of a fixed interval angle 120 deg among them, as shown in Fig. 3c, and they are actuated by the same control gain ($G_1 = G_2 = G_3$) and phase shift ($\sigma_1 = \sigma_2 = \sigma_3$). The effect of the actuator patch area on the control performance is studied by calculating the minimum control gain with different sector angle $\Delta\theta$ of each patch, and the results are shown in Fig. 9a. From Fig. 9a, one can find that the control gain for flutter mode (0, 3) reaches a relative smaller value with the increase of the sector angle and then increases. However, only the flutter mode (0, 3) can be controlled, and the flutter suppression of modes (0, 4) and (0, 5) is disabled for this actuating policy design.

To avoid the limitation on flutter suppression, another actuating policy is suggested, where the control gains for the three actuators have same values as before ($G_1 = G_2 = G_3$); a relative phase shift σ_{123} is assumed among the there phase shifts for the actuator patches, for example, $\sigma_2 = \sigma_1 + \sigma_{123}$, $\sigma_3 = \sigma_2 + \sigma_{123}$. The size of each patch has the same sector angle of $\Delta\theta = 40$ deg/3, such that the total area of the three patches is equal to the optimal size of the one patch case for the aim of comparisons. By adjusting the relative phase shift σ_{123}, the minimum control gains for the flutter suppression of modes from (0, 3) to (0, 5) vary accordingly, which are shown in Fig. 9b. When σ_{123} equals about -160 deg, a better control performance for flutter modes from (0, 3) to (0, 5) is achieved. With comparison to the result of the one-patch case, the minimum control gain is reduced by 28% for the high mode (0, 5), but slightly increases on those of mode (0, 3) or (0, 4). This shows that high control performance, especially for the high flutter mode and multimode suppression, can be obtained by using three actuator patches.

V. Conclusions

A feedback control technique using actuator patches has been developed to suppress flutter of a rotating disk in an air-filled enclosure. The multiple actuator patches can have various configurations in terms of number of patches, the area of individual patch and separation space between the patches. The configurations of actuator patches affect the flutter control performance through altering the control force matrix, which are evaluated by the stability analysis of the disk-enclosure-actuator system for three cases, namely, one patch, two patches, and three patches. The results demonstrate that the control of flutter suppression can in general be obtained by either a single actuator patch or multiple patches. In case of one actuator patch, a better control for all three flutter modes can be achieved when the sector angle is $\Delta\theta = 40$ deg. In case of two/three actuator patches, the optimal study shows that a better control performance

to suppress all three flutter modes, especially for the high flutter modes, can be achieved by manipulating the relative locations of actuator patches and different control phases among them.

Appendix: Evaluations of Matrices

The elements of matrixes $[\boldsymbol{B}]$ and $[\boldsymbol{P}_f]$ are easily gotten as given here:

$$B_{ml} = 2\pi \int_{\kappa}^{1} \left[(\lambda + n)^2 R_{mn}(r) - \mu \nabla_n^4 R_{mn}(r) + \frac{1}{r}\left(r\sigma_r \frac{\mathrm{d}R_{mn}}{\mathrm{d}r} \right) - \frac{n^2}{r^2}\sigma_\theta R_{mn}(r) \right] R_{ln}(r) r \, \mathrm{d}r \tag{A1}$$

$$P_{ml}^{f} = -2\pi \int_{\kappa}^{1} Ci \left[\lambda + \left(1 - \frac{\Omega_d}{\Omega} \right) n \right] R_{mn}(r) R_{ln}(r) r \, \mathrm{d}r \tag{A2}$$

With application of the inner product on Eq. (1) with $R_{ln}(r)e^{in\theta}$, $(l = 0, 1, \ldots, M_0)$, there generate an acoustic force vector $[\boldsymbol{q}_a]$ and a control force vector $[\boldsymbol{q}_c]$ on the right-hand side. The elements for them are, respectively, expressed as

$$q_l^a = 4\pi \int_{\kappa}^{1} \Lambda\lambda i \left[\sum_{k=1}^{\infty} d_k^a \cosh(\alpha_k z_e) J_n(\xi_k r) \right] R_{ln}(r) r \, \mathrm{d}r$$

$$q_l^c = 2\pi \int_{\kappa}^{1} \Lambda\lambda i \left[\sum_{k=1}^{\infty} d_k^c J_n(\xi_k r) \right] R_{ln}(r) r \, \mathrm{d}r \tag{A3}$$

or they are further rewritten in the matrix forms

$$[\boldsymbol{q}_a] = 4\pi \Lambda\lambda i \int_{\kappa}^{1} \{[\boldsymbol{Y}][\boldsymbol{\Phi}_a][\boldsymbol{D}_a]\} r \, \mathrm{d}r$$

$$[\boldsymbol{q}_c] = 2\pi \Lambda\lambda i \int_{\kappa}^{1} \{[\boldsymbol{Y}][\boldsymbol{\Phi}_c][\boldsymbol{D}_c]\} r \, \mathrm{d}r \tag{A4}$$

in which the following vectors are introduced:

$$[\boldsymbol{Y}] = \begin{bmatrix} R_{0n}(r) & R_{1n}(r) & \cdots & R_{M_0 n}(r) \end{bmatrix}^T \tag{A5}$$

$$[\boldsymbol{\Phi}_a] = \begin{bmatrix} \cosh(\alpha_1 z_e) J_n(\xi_1 r) & \cosh(\alpha_2 z_e) J_n(\xi_2 r) & \cdots & \cosh\left(\alpha_{K_0} z_e\right) J_n\left(\xi_{K_0 r}\right) \end{bmatrix}$$

$$[\boldsymbol{\Phi}_c] = \begin{bmatrix} J_n(\xi_1 r) & J_n(\xi_2 r) & \cdots & J_n\left(\xi_{K_0} r\right) \end{bmatrix} \tag{A6}$$

$$[\boldsymbol{D}_a] = \begin{bmatrix} d_1^a & d_2^a & \cdots & d_{K_0}^a \end{bmatrix}^T, \qquad [\boldsymbol{D}_c] = \begin{bmatrix} d_1^c & d_2^c & \cdots & d_{K_0}^c \end{bmatrix}^T \tag{A7}$$

Both $[\boldsymbol{D}_a]$ and $[\boldsymbol{D}_c]$ are related to the disk vibrations, that is, the coefficient $[\boldsymbol{c}]$, through the boundary conditions. Substituting Eqs. (14) and (15) into the match and boundary conditions of Eq. (7b), we have

$$\sum_{k=1}^{K_0} d_k^a \alpha_k \sinh(\alpha_k z_e) J_n(\xi_k r) = 0, \qquad \text{at} \qquad 0 \le r < \kappa$$

$$-\sum_{k=1}^{K_0} d_k^a \alpha_k \sinh(\alpha_k z_e) J_n(\xi_k r) = \sum_{m=0}^{M_0} c_m \lambda i R_{mn}(r), \quad \text{at} \quad \kappa \le r \le 1$$

$$\sum_{k=1}^{K_0} d_k^a \cosh(\alpha_k z_e) J_n(\xi_k r) = 0, \qquad \text{at} \qquad 1 < r \le r_e \tag{A8}$$

We take the finite terms of $k = 1, 2, 3, \ldots, K_0$ for the truncation of the infinite series and choose finite points $r = r_\beta (\beta = 1, 2, 3, \ldots, K_0)$ in the domain of $0 \le r \le r_e$ for approximate satisfaction of Eq. (A8). This leads to a matrix equation as follows:

$$[\boldsymbol{A}_a][\boldsymbol{D}_a] = i\lambda[\boldsymbol{R}_a][\boldsymbol{c}] \tag{A9}$$

in which $[\boldsymbol{A}_a]$ is a $K_0 \times K_0$ matrix

$$[\boldsymbol{A}_a] = \begin{bmatrix} \alpha_1 \sinh(\alpha_1 z_e) J_n(\xi_1 r_1) & \alpha_2 \sinh(\alpha_2 z_e) J_n(\xi_2 r_1) & \cdots & \alpha_{K_0} \sinh\left(\alpha_{K_0} z_e\right) J_n\left(\xi_{K_0} r_1\right) \\ \alpha_1 \sinh(\alpha_1 z_e) J_n(\xi_1 r_2) & \alpha_2 \sinh(\alpha_2 z_e) J_n(\xi_2 r_2) & \cdots & \alpha_{K_0} \sinh\left(\alpha_{K_0} z_e\right) J_n\left(\xi_{K_0} r_2\right) \\ \vdots & \vdots & \ddots & \vdots \\ \alpha_1 \sinh(\alpha_1 z_e) J_n\left(\xi_1 r_{K_0^1}\right) & \alpha_2 \sinh(\alpha_2 z_e) J_n\left(\xi_2 r_{K_0^1}\right) & \cdots & \alpha_{K_0} \sinh\left(\alpha_{K_0} z_e\right) J_n\left(\xi_{K_0} r_{K_0^1}\right) \\ -\alpha_1 \sinh(\alpha_1 z_e) J_n\left(\xi_1 r_{K_0^1+1}\right) & -\alpha_2 \sinh(\alpha_2 z_e) J_n\left(\xi_2 r_{K_0^1+1}\right) & \cdots & -\alpha_{K_0} \sinh\left(\alpha_{K_0} z_e\right) J_n\left(\xi_{K_0} r_{K_0^1+1}\right) \\ \vdots & \vdots & \ddots & \vdots \\ -\alpha_1 \sinh(\alpha_1 z_e) J_n\left(\xi_1 r_{K_0^1+K_0^2}\right) & -\alpha_2 \sinh(\alpha_2 z_e) J_n\left(\xi_2 r_{K_0^1+K_0^2}\right) & \cdots & -\alpha_{K_0} \sinh\left(\alpha_{K_0} z_e\right) J_n\left(\xi_{K_0} r_{K_0^1+K_0^2}\right) \\ \cosh(\alpha_1 z_e) J_n\left(\xi_1 r_{K_0^1+K_0^2+1}\right) & \cosh(\alpha_2 z_e) J_n\left(\xi_2 r_{K_0^1+K_0^2+1}\right) & \cdots & \cosh\left(\alpha_{K_0} z_e\right) J_n\left(\xi_{K_0} r_{K_0^1+K_0^2+1}\right) \\ \vdots & \vdots & \ddots & \vdots \\ \cosh(\alpha_1 z_e) J_n\left(\xi_1 r_{K_0}\right) & \cosh(\alpha_2 z_e) J_n\left(\xi_2 r_{K_0}\right) & \cdots & \cosh\left(\alpha_{K_0} z_e\right) J_n\left(\xi_{K_0} r_{K_0}\right) \end{bmatrix} \tag{A10}$$

and $[\boldsymbol{R}_a]$ is a $K_0 \times (M_0 + 1)$ matrix

$$[\boldsymbol{R}_a] = \begin{bmatrix} 0 & & & \\ \vdots & & & \\ 0 & & & \\ R_{0n}\left(r_{K_0^1+1}\right) & R_{1n}\left(r_{K_0^1+1}\right) & \cdots & R_{M_0 n}\left(r_{K_0^1+1}\right) \\ R_{0n}\left(r_{K_0^1+2}\right) & R_{1n}\left(r_{K_0^1+2}\right) & \cdots & R_{M_0 n}\left(r_{K_0^1+2}\right) \\ \vdots & \vdots & \vdots & \vdots \\ R_{0n}\left(r_{K_0^1+K_0^2}\right) & R_{1n}\left(r_{K_0^1+K_0^2}\right) & \cdots & R_{M_0 n}\left(r_{K_0^1+K_0^2}\right) \\ 0 & & & \\ \vdots & & & \\ 0 & & & \end{bmatrix} \tag{A11}$$

where K_0^1, K_0^2, and $K_0 - K_0^1 - K_0^2$ are the numbers of the discrete points in $0 \le r_\beta < \kappa$, $\kappa \le r_\beta \le 1$, and $1 < r_\beta \le r_e$, respectively.

Solving $[\boldsymbol{D}_a]$ from Eq. (A9) and substituting it into Eq. (A4) yields

$$[\boldsymbol{q}_a] = -4\pi \Lambda\lambda^2 \int_{\kappa}^{1} \{[\boldsymbol{Y}][\boldsymbol{\Phi}_a][\boldsymbol{A}_a]^{-1}[\boldsymbol{R}_a][\boldsymbol{c}]\} r \, \mathrm{d}r = [\boldsymbol{P}_a][\boldsymbol{c}] \tag{A12}$$

where the matrix $[\boldsymbol{P}_a]$ is obtained by

$$[\boldsymbol{P}_a] = -4\pi \Lambda\lambda^2 \int_{\kappa}^{1} \{[\boldsymbol{Y}][\Phi_a][\boldsymbol{A}_a]^{-1}[\boldsymbol{R}_a]\} r \, \mathrm{d}r \tag{A13}$$

A similar procedure can be applied to $[\boldsymbol{q}_c]$ to get

$$[\boldsymbol{D}_c] = i\lambda e^{in\theta_s} [\boldsymbol{A}_c]^{-1} [\boldsymbol{R}_c][\boldsymbol{c}] \tag{A14}$$

and the matrix associated with the control acoustic force is

$$[\boldsymbol{P}_c] = -2\pi\Lambda\lambda^2 e^{in\theta_s}\int_{\kappa}^{1}\{[\boldsymbol{Y}][\Phi_c][\boldsymbol{A}_c]^{-1}[\boldsymbol{R}_c]\}r\,\mathrm{d}r \tag{A15}$$

where

$$[\boldsymbol{A}_c] = \begin{bmatrix} \alpha_1\sinh(\alpha_1 z_e)J_n(\xi_1 r_1) & \alpha_2\sinh(\alpha_2 z_e)J_n(\xi_2 r_1) & \cdots & \alpha_{K_0}\sinh\left(\alpha_{K_0} z_e\right)J_n\left(\xi_{K_0} r_1\right) \\ \alpha_1\sinh(\alpha_1 z_e)J_n(\xi_1 r_2) & \alpha_2\sinh(\alpha_2 z_e)J_n(\xi_2 r_2) & \cdots & \alpha_{K_0}\sinh\left(\alpha_{K_0} z_e\right)J_n\left(\xi_{K_0} r_2\right) \\ \vdots & \vdots & \ddots & \vdots \\ \alpha_1\sinh(\alpha_1 z_e)J_n\left(\xi_1 r_{K_0}\right) & \alpha_2\sinh(\alpha_2 z_e)J_n\left(\xi_2 r_{K_0}\right) & \cdots & \alpha_{K_0}\sinh\left(\alpha_{K_0} z_e\right)J_n\left(\xi_{K_0} r_{K_0}\right) \end{bmatrix} \tag{A16}$$

$$[\boldsymbol{R}_c] = \begin{bmatrix} a_n(r_1)R_{0n}(r_s) & a_n(r_1)R_{1n}(r_s) & \cdots & a_n(r_1)R_{M_0 n}(r_s) \\ a_n(r_2)R_{0n}(r_s) & a_n(r_2)R_{1n}(r_s) & \cdots & a_n(r_2)R_{M_0 n}(r_s) \\ \vdots & \vdots & \ddots & \vdots \\ a_n\left(r_{K_0}\right)R_{0n}(r_s) & a_n\left(r_{K_0}\right)R_{1n}(r_s) & \cdots & a_n\left(r_{K_0}\right)R_{M_0 n}(r_s) \end{bmatrix} \tag{A17}$$

in which

$$a_n(r) = \sum_{j=1}^{J} a_{jn}(r)$$

is a generalized function of the Fourier expansion coefficients $a_{jn}(r)$ for the distribution function $A_j(r,\theta)$ $(j = 1, 2, \ldots, J)$ of the actuator patches.

Acknowledgments

The authors acknowledge the finance support provided by Lanzhou University and the Center for Mechanics of Micro-System of Nanyang Technological University.

References

[1]Hosaka, H., and Crandall, S. H., "Self-Excited Vibrations of a Flexible Disk Rotating on an Air Film Above a Flat Surface," *Acta Mechanica*, Vol. 3, No. 1, 1992, pp. 115–127.

[2]Huang, F., and Mote, C. D., Jr., "On the Instability Mechanism of a Disk Rotating Close to a Rigid Surface," *Journal of Applied Mechanics*, Vol. 62, No. 6, 1995, pp. 764–771.

[3]Renshaw, A. A., "Critical Speeds for Floppy Disks," *Journal of Applied Mechanics*, Vol. 65, No. 2, 1998, pp. 116–120.

[4]Yasuda, K., Torii, T., and Shimizu, T., "Self-Excited Oscillations of a Circular Disk Rotating in Air," *JSME International Journal*, Vol. 35, No. 3, 1992, pp. 347–352.

[5]D'angelo, C., and Mote, C. D., Jr., "Aerodynamically Excited Vibration and Flutter of a Thin Disk Rotating at Supercritical Speed," *Journal of Sound and Vibration*, Vol. 168, No. 1, 1993, pp. 15–30.

[6]Renshaw, A. A., D'angelo, C., and Mote, C. D., Jr., "Aerodynamically Excited Vibration of a Rotating Disk," *Journal of Sound and Vibration*, Vol. 177, No. 5, 1994, pp. 577–590.

[7]Kim, B. C., Raman, A., and Mote, C. D., Jr., "Prediction of Aeroelastic Flutter in a Hard Disk Drive," *Journal of Sound and Vibration*, Vol. 238, No. 2, 2000, pp. 309–325.

[8]Hansen, M. H., Raman, A., and Mote, C. D., Jr., "Estimation of Nonconservative Aerodynamic Pressure Leading to Flutter of Spinning Disks," *Journal of Fluids and Structures*, Vol. 15, No. 1, 2001, pp. 39–57.

[9]Imai, S., Tokuyama, M., and Yamaguchi, Y., "Reduction of Disk Flutter by Decreasing Disk-to-Shroud Spacing," *IEEE Transactions on Magnetics*, Vol. 35, No. 5, 1999, pp. 2301–2303.

[10]Imai, S., "Fluid Dynamics Mechanism of Disk Flutter by Measuring the Pressure Between Disks," *IEEE Transactions on Magnetics*, Vol. 37, No. 2, 2001, pp. 837–841.

[11]Heo, B., Shen, I. Y., and Riley, J. J., "Reducing Disk Flutter by Improving Aerodynamic Design of Base Castings," *IEEE Transactions on Magnetics*, Vol. 36, No. 5, 2000, pp. 2222–2224.

[12]Bittner, H., and Shen, I. Y., "Taming Disk/Spindle Vibrations Through Aerodynamic Bearings and Acoustically Tuned-Mass Dampers," *IEEE Transactions on Magnetics*, Vol. 35, No. 2, 1999, pp. 827–832.

[13]Deeyiengyang, S., and Ono, K., "Suppression of Resonance Amplitude of Disk Vibration by Squeeze Air Bearing Plate," *IEEE Transactions on Magnetics*, Vol. 37, No. 2, 2001, pp. 820–825.

[14]Huang, X. Y., Wang, X., and Yap, F. F., "Feedback Control of Rotating Disk Flutter in an Enclosure," *Journal of Fluids and Structures*, Vol. 19, No. 7, 2004, pp. 917–932.

[15]Huang, X. Y., Hoque, M. E., and Wang, X., "An Experimental Study on Feedback Control of Rotating Disk Flutter," *Journal of Fluids and Structures*, Vol. 20, No. 1, 2005, pp. 71–80.

[16]Sokolnikoff, I. S., *Mathematical Theory of Elasticity*, 2nd ed., McGraw–Hill, New York, 1956.

[17]Chonan, S., Mikami, T., and Ishikawa, H., "The Vibration and Critical Speeds of Rotating Sawblades," *Proceedings of JSME, Part C*, Vol. 52, No. 12, 1985, pp. 1805–1812 (in Japanese).

M. Ahmadian
Associate Editor